DALTON
FULL PAPER

An unusual phase transition in the crystal structure and physical properties of $(TTF)_9[Mo(CN)_8]_2 \cdot 4H_2O$, where TTF = tetrathiafulvalene

Guillaume Rombaut,[a] Scott S. Turner,*[b] Delphine Le Pévelen,[b,c] Corine Mathonière,*[a] Peter Day[b] and Keith Prout[c]

[a] *Laboratoire des Sciences Moléculaires, Institut de Chimie de la Matière Condensée de Bordeaux, Avenue du Dr A. Schweitzer, 33608 Pessac cedex, France*
[b] *Davy-Faraday Research Laboratory, Royal Institution of Great Britain, 21 Albemarle Street, London, UK W1S 4BS*
[c] *Chemical Crystallography Laboratory, University of Oxford, 9 Parks Road, Oxford, UK OX1 3PD*

Received 13th June 2001, Accepted 24th September 2001
First published as an Advance Article on the web 26th October 2001

At 270 K, the charge transfer salt $(TTF)_9[Mo(CN)_8]_2 \cdot 4H_2O$, **I**, crystallizes in the triclinic space group $P\bar{1}$ with $a = 9.9094(2)$, $b = 10.6781(2)$, $c = 23.6086(7)$ Å, $\alpha = 75.7910(8)$, $\beta = 88.6010(9)$, $\gamma = 78.5250(8)°$, $V = 2372.5(1)$ Å^3 and $Z = 2$. At 120 K, the space group is unchanged with $a = 9.7990(7)$, $b = 10.6630(5)$, $c = 22.9940(2)$ Å, $\alpha = 79.981(4)$, $\beta = 89.798(4)$, $\gamma = 79.013(4)°$, $V = 2321.5$ Å^3 and $Z = 2$. On comparing the two sets of data, we see significant changes in the cell parameters, most notably in the angle α. Variable temperature crystallographic studies indicate a first order phase transition accompanied by hysteresis, which corresponds to a change in the transport properties. **I** is a semiconductor and the high temperature activation energy of 0.06 eV changes sharply to 0.15 eV below 236 K. Bulk magnetic susceptibility and ESR measurements indicate that the TTF molecules are antiferromagnetically coupled. The temperature dependence of the EPR spectrum changes from 300–200 K, in approximate agreement with the transport and structural results. The optical spectrum of $(TTF)_9[Mo(CN)_8]_2 \cdot 4H_2O$ consists of several broad bands assigned to TTF charged molecules, to $[Mo(CN)_8]^{4-}$ and to charge transfer from the donors to the acceptor in the near infra-red range. Preliminary magnetic susceptibility measurements under light irradiation with a multi-line (752.5–799.3 nm) laser were also performed, but no photomagnetic effect was noted.

Introduction

The development of radical cation salts based on planar π-electron donors, such as tetrathiafulvalene (TTF), is continuing to attract considerable interest, since they provide materials with a remarkable variety of structures and transport properties.[1–3] One of the most exciting challenges is to prepare molecular based compounds with the potential to display a synergy between two or more physical properties, or that have properties which are difficult to obtain otherwise. Typically, this is attempted by using electronically 'non-innocent' counterions that also have a useful property, such as ferromagnetism or spin transition. For example, the bis(ethylenedithio)tetrathiafulvalene, BEDT-TTF, salt of $[MnCr(C_2O_4)_3]^-$ shows long range ferromagnetic order below $T_c = 5.5$ K due to the anion and simultaneous metallic conduction because of the organic network.[4–6] Furthermore, some of us have synthesised a number of BEDT-TTF and TTF salts that incorporate anion···cation π-stacking, which promotes long range ferrimagnetic order with T_c's between 4.2 and 9 K.[7,8] Most recent developments have focussed on designing materials that combine conducting and magnetic properties and there have been a few attempts to introduce anions that have photophysical properties or unusual structural transitions. This is with a view to obtaining molecular conductors in which the transport properties could be altered by an external and easily controllable stimulus, *i.e.* light. For example, both TTF and BEDT-TTF salts of the photochromic nitroprusside anion, $[Fe(CN)_5NO]^{2-}$, are known,[9,10] although so far no light-activated changes in the conductivity have been reported despite the fact that the anion exhibits a photoinduced transition to a long-lived metastable state below 160 K.[11]

Another group of anions that are good candidates to promote photophysical effects in conductors are the octacyanometallate anions of the transition metals Mo(IV, V) or W(IV, V) as they have been well studied from the point of view of their structure and photochemistry.[12] Some of us have shown that the intrinsic susceptibility to photooxidation of Mo(IV) with $S = 0$ to Mo(V) with $S = 1/2$ is maintained in the solid state, by irradiation in the UV range.[13] Furthermore, the flexibility of the oxidation state allowed us to obtain compounds that present intervalence bands in the optical spectrum, due to electronic delocalisation.[14] These properties allowed us to observe photomagnetic effects in polymetallic networks with a SQUID detector.[13,14] In our continuing efforts to obtain multi-property materials, we present the synthesis and characterisation of the first TTF based charge transfer salt of the photoactive $[Mo^{IV}(CN)_8]^{4-}$ anion.

Experimental

Synthesis

$K_4[Mo^{IV}(CN)_8] \cdot 2H_2O$[15] was prepared following the published method. All solvents were freshly distilled immediately before use. The electrochemical cell and electrodes were washed with

 DOI: 10.1039/b105212h

nitric acid followed by distilled water and thoroughly dried at 160 °C.

$(TTF)_9[Mo^{IV}(CN)_8]_2\cdot 4H_2O$, I. The charge transfer salt was prepared by *in situ* oxidation of 10 mg TTF placed in the anode arm of an H-shaped electrochemical cell (total volume 50 ml). The cell had two glass frits, in the H-cross-bar and in the cathode arm, which prevented contamination by reduction products. The remainder of the cell was filled with a filtered solution of $K_4[Mo^{IV}(CN)_8]\cdot 2H_2O$ (80 mg) in a mixture of H_2O (25 ml) and acetone (25 ml). A constant current of 1 μA was applied across the cell for one week, giving a relatively large quantity of dark brown crystals with a needle morphology and a small amount of dark coloured blocks. Further investigation revealed that the major needle phase was promoted when a higher percentage of acetone was used and the optimum yield of needles was found for the solvent mixture 35 ml acetone and 15 ml H_2O. The needle phase crystals, which were suitable for structure solution by X-ray single crystal diffraction, had stoichiometry $(TTF)_9[Mo(CN)_8]_2\cdot 4H_2O$. Elemental analysis found for needle phase: C 32.9, H 1.5, N 8.93, S 45.6, Mo 7.2; calc. for $C_{70}H_{44}N_{16}S_{36}O_4Mo_2$, C 33.3, H 1.88, N 8.88, S 45.8, Mo 7.6%.

The block phase, as prepared above, has so far proven difficult to characterise. On replacing TTF with the donors BEDT-TTF, bis(ethylenedithio)tetrathiafulvalene, or TMTSF, tetramethyltetraselenafulvalene, no solid formed on the anode after three weeks. Similarly, electrocrystallisation with $K_4[W^{IV}(CN)_8]$ also produced no solid. No product was obtained even after raising the constant current to 3–5 μA.

Physical measurements

Magnetic susceptibility measurements were carried out with a Quantum Design MPMS-5S SQUID magnetometer working in dc mode down to a temperature of 2 K and in an applied field range up to 5 T. The diamagnetic corrections were estimated using Pascal's constants. Photomagnetic experiments were performed with a Kr laser coupled with an optical fibre directed into the SQUID cavity. Transmission infra-red spectra were recorded by a Perkin-Elmer FT-IR Paragon 1000 spectrometer from KBr pellets; the optical spectra by a CARY 5E spectrophotometer equipped with a diffusion sphere. EPR spectra were measured with a Bruker EMX spectrometer operating at X-band (*ca.* 9.46 GHz) equipped with an Oxford Instruments ESR-900 flowing-helium cryostat (4.2–300 K) and controlled by an Oxford Instruments ITC4 temperature control unit. Four probe dc transport measurements were made with an Oxford Instruments MagLab 2000 equipped with an EP probe, operating from 2–350 K. Gold wire electrodes (0.025 mm diam.) were attached directly to the crystal surface using Au paste.

The X-ray diffraction measurements where performed on a Nonius κ-CCD for the 270 K data and on an Enraf Nonius Dip 2020 diffractometer with imaging plate detector for the 120 K data set. Both used graphite-monochromated Mo-Kα radiation (0.71073 Å). The structures were solved using direct methods with SIR 97[16] and refined by using CRYSTALS 2000.[17] For both temperatures, the Mo, S, O and N atoms were refined anisotropically, whereas the C atoms were refined isotropically. At 270 K, the hydrogen atoms of the TTF and the water molecules (except for O47, for which hydrogen atoms were found using a Fourier map) were positioned on the basis of geometrical considerations and were not refined. At 120 K, the positions of the hydrogen atoms of both water molecules were found using a Fourier difference map and these positions have been refined. The hydrogen atoms of the TTF molecules were positioned on the basis of geometrical considerations and were not refined.

CCDC reference numbers 165777 and 165778.

See http://www.rsc.org/suppdata/dt/b1/b105212h/ for crystallographic data in CIF or other electronic format.

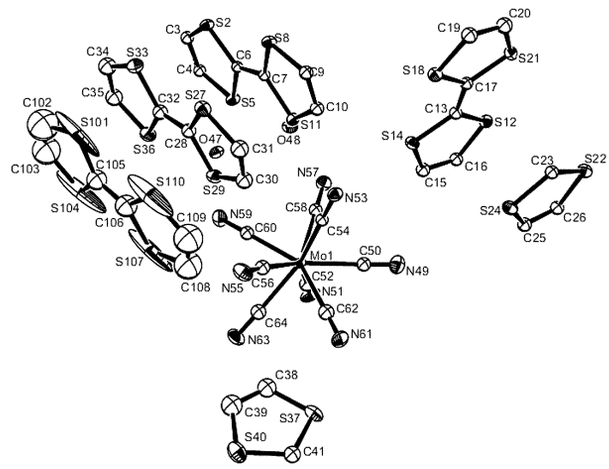

Fig. 1 Standard ORTEP[18] diagram for $(TTF)_9[Mo(CN)_8]_2\cdot 4H_2O$ with the atom numbering scheme and 50% thermal ellipsoids. Hydrogen atoms have been omitted for clarity.

Results and discussion

Crystal structures

The crystal data and collection parameters for the structures described below are given in Table 1. The crystals with needle morphology were suitable for single crystal structure analysis and the resulting data were solved as $(TTF)_9[Mo(CN)_8]_2\cdot 4H_2O$, **I**. At both experimental temperatures, 270 and 120 K, one of the TTF molecules was found to be highly disordered. For this disordered molecule, the positions of the atoms were found using a Fourier difference map and then refined using restraints on the bond lengths. However, the model obtained is not completely satisfactory, since the thermal ellipsoids of the S atoms are strongly elongated. Attempts to position the TTF over two sites or more do not lead to any improvement in the agreement with the experimental data.

A phase change occurs between 270 and 120 K, accompanied by a significant change in the a cell parameter from the high temperature phase, HT, with $a = 75.7910(8)°$ to the low temperature phase, LT, with $a = 79.981(4)°$. Lattice contraction with decreasing temperature changes the other cell parameters, but to a much lesser extent. Thus, the change from 270 to 120 K is approximately 0.7% for parameter a, 0.1% for b, 2.1% for c and 5.2, 1.3 and 0.7% for parameters α, β and γ, respectively.

The phase change is associated with a change in the spatial relationship between neighbouring TTF molecules along the crystallographic b axis (corresponding to the long axis of the needles) and this is described in more detail below. Diffraction data collected on cooling and warming through the phase transition temperature at 2 K min^{-1} reveal hysteresis behaviour. On cooling, only the HT phase is present at 278 and 270 K, but at 260 K, the LT phase begins to appear and the transition is complete at 245 K. With subsequent warming, the LT phase persists exclusively up to 255 K, and at 260 K the HT phase begins to appear and is the only phase apparent at 275 K and above. From crystallographic data, the hysteresis is therefore about 10 K (255 to 265 K).

Fig. 1 is a standard ORTEP[18] diagram of the asymmetric unit of **I** at 120 K, with the atom numbering scheme and 50% thermal ellipsoids. The molecule that contains atoms numbered 101 to 110 is clearly the disordered TTF. As in the majority of charge transfer salts of this type, both the LT and HT phases consist of discrete layers of donor molecules and anions although the structures are not simple alternations of ions as found in most BEDT-TTF salts.[1–3] The overall layered structure can be seen from the packing diagram projected along the a direction, shown in Fig. 2. It consists of three repeating layers, labelled A to C in Fig. 2. Layer A contains only donors and

Table 1 Crystallographic data for $(TTF)_9[Mo(CN)_8]_2 \cdot 4H_2O$

Compound	**I** (HT phase)	**I** (LT phase)
Empirical formula	$C_{35}H_{22}MoN_8O_2S_{18}$	$C_{35}H_{22}MoN_8O_2S_{18}$
Formula weight	1259.64	1259.64
T/K	270(1)	120(1)
Wavelength/Å	0.71069 (Mo-Kα)	0.71069
Crystal system	Triclinic	Triclinic
Space group	$P\bar{1}$ (no. 2)	$P\bar{1}$
a/Å	9.9094(2)	9.799(1)
b/Å	10.6781(2)	10.663(1)
c/Å	23.6086(2)	22.994(2)
α/°	75.7910(8)	79.981(4)
β/°	88.6010(9)	89.798(4)
γ/°	78.5250(8)	79.013(4)
V/Å^3	2372.5(1)	2321.5(3)
Z	2	2
ρ_{calc}/Mg m^{-3}	1.763	1.802
μ/mm^{-1}	1.114	1.138
F(000)	1268	1268
Final R indices	$R1 = 0.0441$, $wR2 = 0.0451$, $I > 3\sigma$	$R1 = 0.0484$, $wR2 = 0.0316$, $I > 5\sigma$

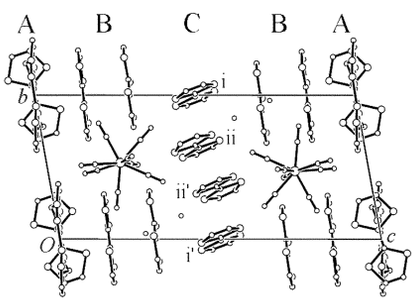

Fig. 2 Packing diagram for $(TTF)_9[Mo(CN)_8]_2 \cdot 4H_2O$ as viewed along the crystallographic a axis.

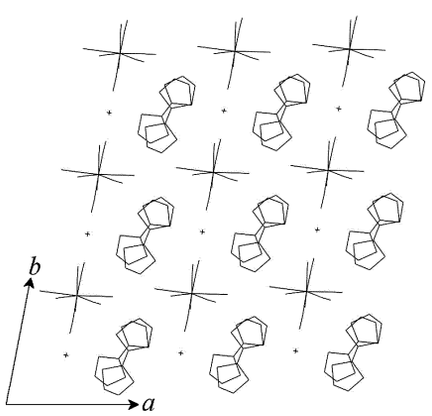

Fig. 3 Packing diagram for $(TTF)_9[Mo(CN)_8]_2 \cdot 4H_2O$ of the layer that contains the anion, as viewed along the crystallographic c axis.

includes the disordered TTF molecule. Layer B contains alternating $[Mo(CN)_8]^{4-}$ anions and TTF dimers, which lie perpendicular to the third layer, C, consisting of a stack of donors parallel to the b axis. The three layers are repeated in the pattern ABCBAB, *etc.* Layer B is shown in more detail in Fig. 3, where the O atoms from the H_2O are situated in cavities bound by the anions and TTF dimers. The remaining H_2O molecules lie between layers B and C and show significant disorder in the b direction at 270 K. The oxygen atom is delocalised over two sites, one with an occupancy factor of ~75%, and the other with an occupancy factor of ~25%. At low temperature, this disorder does not exist.

The most pronounced differences between the HT and LT phases occur in layer C in the relative positions of the TTF molecules i and ii, and ii and ii′, according to the labelling scheme in Fig. 2. The difference between the two phases is further highlighted in Fig. 4, which shows views of four sets of

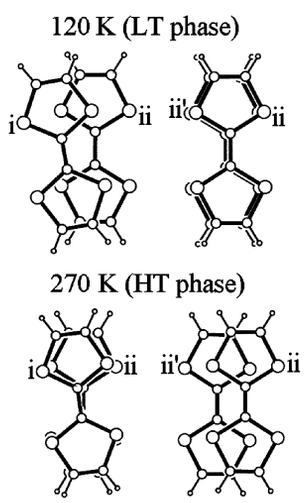

Fig. 4 The relationships between TTF molecules in the one dimensional donor stack at 120 and 270 K.

TTF pairs: those at the top are from the LT phase and those at the bottom from the HT phase. The relationship between TTF molecules i and ii is shown on the left, and ii and ii′ on the right, the labelling being the same as in Fig. 2. The projections in Fig. 4 are standardised to be perpendicular to the mean plane of TTF molecule ii. For both the HT and LT phases, layer C contains numerous close S···S contacts below the van der Waals sum of 3.6 Å, which are modified at the phase transition. Between S atoms within the TTF stacks, the shortest atomic contact at 120 K is 3.392(2) Å between S14 and S21, that is, between molecules ii and ii′. However, at 270 K the distance between the same atoms has lengthened to 3.823(2) Å, which is the shortest distance between molecules ii and ii′ at this temperature. Also at 270 K, the shortest overall S···S contact is 3.500(2) Å between molecules i and ii (S18 and S22). In the LT phase, this distance increases to 3.752(2) Å. Other intra-stack contacts are found at 120 K between S18···S12 at 3.423(2) Å, S21···S24 at 3.667(2) Å, S12···S24 at 3.715(2) Å and S12···S22 at 3.749 (2) Å. At 270 K, these contacts are respectively 3.847(2), 3.525(2), 4.317(2) and 3.535(2) Å. The remaining short contact at 270 K is S14···S24, which is 3.540(2) between molecules i and ii (this contact is 3.858 (2) Å at 120 K). Between the donor dimers in layer B there are extremely short S···S contacts which change little with temperature: at 120/270 K, S11···S29 is 3.280(2)/3.298(2) Å, S2···S33 is 3.341(2)/3.363(2) Å, S8···S27 is 3.363(2)/3.383(2) Å and S5···S36 is 3.374(2)/3.378(2) Å. This strongly suggests that the dimers are electronically coupled. Layer A contains no donor–donor short

Table 2 Charges calculated from bond length analysis for $(TTF)_9[Mo(CN)_8]_2 \cdot 4H_2O$. The TTF molecules are identified by referring to the atoms in the central C=C bond

C=C bond	$Q \pm 0.1$, 270 K	$Q \pm 0.1$, 120 K
C13–C17	+0.5	+1.0
C23–C23	+0.7	+0.2
C6–C7	+1.2	+1.1
C28–C32	+0.7	+0.8
C41–C41	+1.1	+1.0
C105–C106	Disordered (+0.7)	Disordered (+0.7)
Total/per Mo	+4.0 ± 0.4	+4.2 ± 0.4

contacts and the most comprehensive continuous S···S network is, therefore, in the crystallographic *b* direction along the infinite stack of TTF molecules. Such a one-dimensional network, formed from donor face to face interactions alone should lead to highly anisotropic electronic transport. The charges on the TTF molecules were estimated from the C=C and C–S bond lengths using a method originally devised for BEDT-TTF salts.[19] For the present study a survey of twenty-three TTF salts produced a linear equation for the calculated charge of $Q = 6.425–7.640\delta$, where δ is defined in the same way as in the BEDT-TTF survey. As expected, the charges resulting from these calculations were very similar, although not identical, to those obtained from the corresponding equation for BEDT-TTF salts. Table 2 shows the calculated charges at both temperatures for the TTF molecules in the asymmetric unit. The TTF molecules that contain C23 or C13 are present in layer C as molecules i and ii, respectively, while those containing C6 or C28 are the dimers present in layer B. Even taking into consideration a 10% error in the calculations, there is clearly charge transfer on decreasing the temperature. In particular, this occurs within the TTF stacks, which may explain the two stage electrical properties described below and the temperature dependence of the magnetic properties. The calculated total charges are consistent with all the Mo centres having the +4 oxidation state, or possibly a +4-dominated mixture of the +5 and +4 states. From this analysis it is not possible that all or most of the Mo centres are in the +5 oxidation state, since that would require a total positive charge closer to +3 per Mo centre, less than that calculated in Table 2.

Infrared and UV-visible spectroscopy

The IR spectrum of the present compound is similar to those of other TTF radical cation double salts. Several vibrational peaks arise from the ν(CN) mode of the $[Mo^{IV}(CN)_8]^{4-}$ anion, as expected.[20]

The UV-visible reflection spectrum of the title compound shows two broad bands at 380 and 540 nm. There is also a further band with a maximum just below 800 nm, which is present as a shoulder on the 540 nm band. The band at 380 nm is associated with charged TTF molecules and ligand field transitions within the $[Mo^{IV}(CN)_8]^{4-}$ anion,[21] while the one at 540 nm must originate from the $TTF^{\bullet+}$ radical cations. In the low energy part of the spectrum, the broad band corresponds to charge transfer between the inorganic $[Mo^{IV}(CN)_8]^{4-}$ donors and organic $TTF^{\bullet+}$ acceptors and is characteristic of ion pairing.[22]

Transport measurements

Variable temperature four probe dc resistance measurements were carried out on several single crystals in the most conductive direction, namely, parallel to the long axis of the needles. In this direction, the room temperature conductivity is 2.67×10^{-3} ohm^{-1} cm^{-1}, which is typical of a semiconductor. This assignment is confirmed by plotting ln(conductivity) against $1000/T$ (Fig. 5), which displays two straight lines with

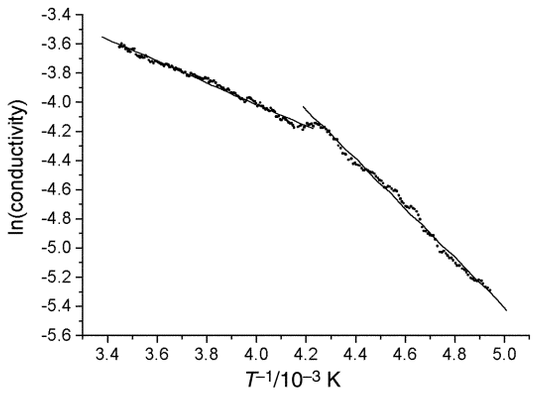

Fig. 5 Plot of ln(conductivity) *versus* inverse temperature (filled circles) and straight line fits to the distinct semiconducting regimes for $(TTF)_9[Mo(CN)_8]_2 \cdot 4H_2O$.

distinctly different gradients corresponding to two different semiconducting activation energies. From 290 and 238 K, the activation energy is 0.06 eV, and between 235 and 202.3 K, it is 0.15 eV, both of which are in the region of values found for BEDT-TTF semiconductors. From the crystal structure, a strong anisotropy in the conductivity would be expected and, indeed, perpendicular to the long axis of the needle two probe resistance measurements gave a room temperature conductivity of 6.51×10^{-5} ohm^{-1} cm^{-1}, which is at the lower end of the range expected for a semiconductor.[23]

Magnetic and preliminary photomagnetic properties

The magnetic properties of **I** were measured on a polycrystalline sample in the temperature range 2–300 K in a magnetic field of 5 kOe. The susceptibility contains only a very weak contribution from the organic sublattice (less than one electron per formula unit) with a $\chi_M T$ value of 0.21 emu K mol^{-1} at room temperature. The $\chi_M T$ product, χ_M being the molar susceptibility and T the temperature, decreases with decreasing temperature, indicating that the TTF radicals are antiferromagnetically coupled. This is in agreement with the crystal structure, which shows very short contacts between charged TTF molecules, leading to some dimerisation as the temperature is lowered.[24]

In an attempt to observe charge transfer between donors and acceptors, we irradiated **I** with light (λ = 752.5–799.3 nm) corresponding to the energy of the ion pairing band described above. The magnetization at 10 K was followed under light irradiation over 10 h but no photomagnetic effect was seen. However, this result does not necessarily indicate that a photo-induced electron transfer does not occur. In fact, if this did happen, the $[Mo^{IV}(CN)_8]^{4-}$ ($S = 0$) would be photo-oxidised to $[Mo^{V}(CN)_8]^{3-}$ ($S = 1/2$) and one spin would be added to the large organic network. Of course this corresponds simply to a relocalisation of the magnetic centers and, since the Mo ion and TTF centres are well separated, no magnetic interactions should be seen.

EPR spectroscopy

For **I**, the lineshape of the EPR varies when the temperature is lowered. Since the $[Mo^{IV}(CN)_8]^{4-}$ anion is diamagnetic, the signal is only due to the presence of spins localised on the TTF radical cations. From 290 to 200 K, both the *g* value and the peak to peak linewidth, ΔH_{pp}, vary markedly (Fig. 6 and 7) ranging from 2.0020 to 2.0064 for $\langle g \rangle$ and 15.94 to 17.01 G for ΔH_{pp}. These changes correlate to the first order phase transition observed in the crystallographic study and transport measurements. On the other hand, the shape of the EPR spectrum does not change further between 200 and 20 K, indicating that there is no change in the electronic motion in the organic network in this temperature range. Below 20 K the spectra become strongly

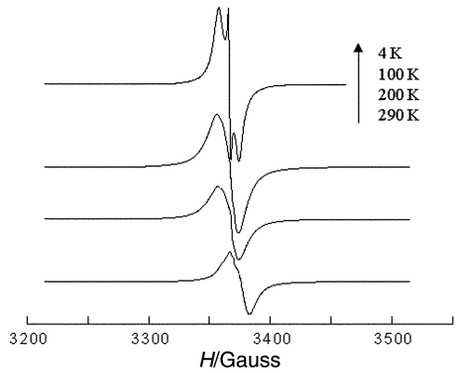

Fig. 6 Temperature dependence of the EPR spectra of a polycrystalline sample of $(TTF)_9[Mo(CN)_8]_2{\cdot}4H_2O$.

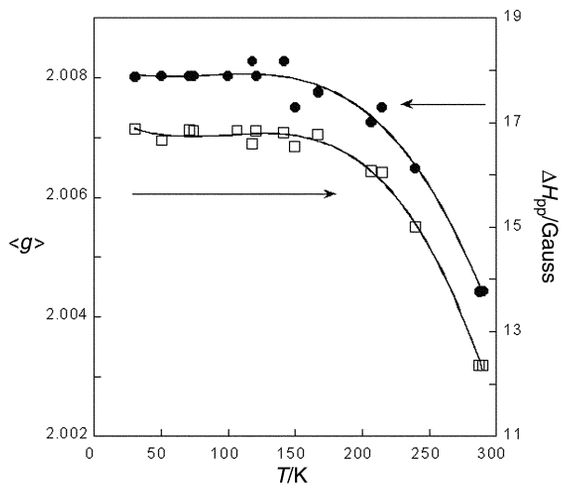

Fig. 7 Temperature dependence of peak to peak band width, ΔH_{pp} (filled circles) and average g values, $\langle g \rangle$ (open squares), for $(TTF)_9[Mo(CN)_8]_2{\cdot}4H_2O$.

anisotropic and characteristic of localised spin on a TTF radical cation with $g_x = 2.0132$, $g_y = 2.0075$ and $g_z = 2.0027$ ($\langle g \rangle = 2.0078$).[25] Furthermore, when plotted *versus* temperature, the double integral of the signal (directly related to the magnetic susceptibility) multiplied by the temperature (DI*T) decreases when the temperature decreases. This behaviour confirms the antiferromagnetic interactions between the charged TTF molecules (Fig. 8)

Conclusion

We have described the synthesis, crystal structure and magnetic and transport properties of a new charge transfer salt with stoichiometry $(TTF)_9[Mo(CN)_8]_2{\cdot}4H_2O$. Variable temperature crystallography indicates that there is a phase change centred about 255 to 265 K which shows hysteresis. In both phases, the structure of this material contains a stack of TTF molecules leading to a one dimensional network of S···S contacts in the crystallographic *b* direction, which corresponds to the long axis of the needle crystals. The crystallographic results show that the largest change between the phases concerns the charge distribution and spatial organisation within this TTF stack. Conductivity measurements of this semiconductor along the long axis of the needles show a corresponding variation in the measured activation energy between the two phases. It is clearly of interest to investigate the variable temperature phase changes and subsequent changes in the physical properties for similar salts. Furthermore, since the anion $[Mo(CN)_8]^{4-}$ is a photosensitive molecular unit, there is an opportunity to alter the charge distribution throughout the molecule with light, thus producing a material in which the physical properties are

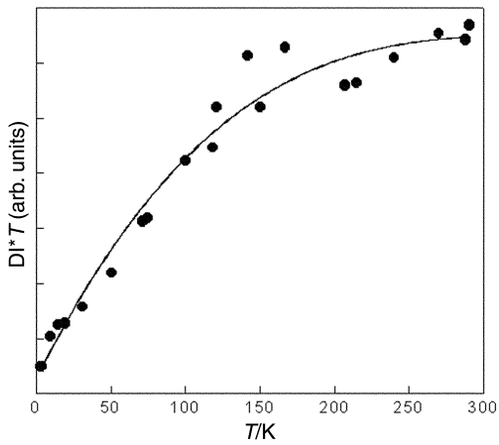

Fig. 8 Double integral of the EPR signal multiplied by temperature (DI*T) *versus* temperature.

changeable. Preliminary bulk magnetic measurements, which were measured under light irradiation, do not reveal any noticeable effect, but evidence would most likely be observed by investigating the conductivity or EPR spectrum before, during and after irradiation. We are continuing our efforts in this direction.

Acknowledgements

This work was supported by the French Centre National de la Reserche Scientifique and the UK Engineering and Physical Sciences Research Council. We would also like to acknowledge the European Commission for Training and Mobility of Researchers and European Network on Molecular Magnetic Materials. We also thank Dr A. Cowley from the Chemical Crystallography Laboratory for fruitful discussions.

References

1 M. Metzger, P. Day and G. C. Papavassiliou, *Lower-Dimensional Systems and Molecular Electronics*, Plenum Press, New York, 1990.
2 J. M. Williams, J. R. Ferraro, R. J. Thorn, K. D. Carlson, U. Geiser, H. H. Wang, A. M. Kini and M. H. Whangbo, *Organic Superconductors (Including Fullerenes): Synthesis, Structure, Properties and Theory*, Prentice Hall, Englewood Cliffs, NJ, 1992.
3 T. Ishiguro, K. Yamaji and G. Saito, *Organic Superconductors*, Springer, Berlin, 2nd edn., 1998.
4 E. Coronado, J. R. Galan-Mascaros and C. J. Gomez-Garcia, *Mol. Cryst. Liq. Cryst. Sci. Technol., Sect. A*, 1999, **334**, 679.
5 F. Berezovsky, S. Trike, J. S. Pala, J. R. Galan-Mascaros and C. J. Gomez-Garcia, *Synth. Met.*, 1999, **102**, 1753.
6 E. Coronado, J. R. Galán-Mascaros, C. J. Gomez-Garcia and V. Laukhin, *Nature*, 2000, **408**, 447.
7 S. S. Turner, D. Le Pevelen, P. Day and K. Prout, *J. Chem. Soc., Dalton Trans.*, 2000, 2739.
8 S. S. Turner, C. Michaut, S. Durot, P. Day, T. Gelbrich and M. B. Hursthouse, *J. Chem. Soc., Dalton Trans.*, 2000, 905.
9 M. Clemente-León, E. Coronado, J. R. Galán-Mascarós, C. J. Gómez-Garcia and E. Canadell, *Inorg. Chem.*, 2000, **39**, 5394.
10 H. Yu and D. Zhu, *Physica C*, 1997, **282**, 1893; M. Gener, E. Canadell, S. S. Khasanov, L. V. Zorina, R. P. Shibaeva, L. A. Kushch and E. B. Yagubskii, *Solid State Commun.*, 1999, **111**, 329; L. A. Kushch, L. Buratov, V. Tkacheva, E. Yagubskii, L. Zorina, S. Khasanov and R. Shibaeva, *Synth. Met.*, 1999, **102**, 1646.
11 U. Hauser, V. Oestreich and H. D. Rohrweck, *Z. Phys. A*, 1977, **17**, 280; Th. Woike, W. Krasser, P. S. Bechthold and S. Haussühl, *Phys. Rev. Lett.*, 1984, **53**, 1767; M. D. Carducci, D. V. Formitchev and P. Coppens, *J. Am. Chem. Soc.*, 1997, **119**, 2669.
12 A. Samotus and J. Szklarzewicz, *Coord. Chem. Rev.*, 1993, **125**, 63.
13 G. Rombaut, S. Golhen, L. Ouahab, C. Mathonière and O. Kahn, *J. Chem. Soc., Dalton Trans.*, 2000, 3609.
14 G. Rombaut, M. Verelst, S. Golhen, L. Ouahab, C. Mathionière and O. Kahn, *Inorg. Chem.*, 2001, **40**, 1151.
15 J. G. Leipoldt, L. D. C. Bok and P. J. Cilliers, *Z. Anorg. Allg. Chem.*, 1974, **409**, 343.

16 A. Altomare, G. Cascarano, C. Giacovazzo, A. Guagliardi and A. G. G. Moliterni, SIR97, Instituto di Ricerca per lo Sviluppo di Metodologie Cristallografiche, Campus Universitario, Bari, Italy, 1997.
17 D. J. Watkin, C. K. Prout, J. R. Carruthers, P. W. Betteridge and R. I. Cooper, CRYSTALS 2000, Issue 11, Chemical Crystallography laboratory, Oxford, UK, 1999.
18 C. K. Johnson, ORTEP, Report ORNL-5138, Oak Ridge National Laboratory, Oak Ridge, TN, 1976.
19 P. Guionneau, C. J. Kepert, D. Chasseau, M. R. Truter and P. Day, *Synth. Met.*, 1997, **86**, 1973.
20 K. O. Hartman and F. A. Miller, *Spectrochim. Acta, Part A*, 1968, **24**, 669.
21 J. R. Perumareddi, A. Liehr and A. W. Adamson, *J. Am. Chem. Soc.*, 1963, **85**, 249.
22 A. Mhanni, L. Ouahab, O. Pena, C. Garrigou-Lagrange and P. Delhaes, *Synth. Met.*, 1991, **41–43**, 1703.
23 A. R. West, *Solid State Chemistry and its Applications*, John Wiley and Sons, New York, 1995.
24 M. Clemente-León, E. Coronado, J. R. Galán-Mascarós, C. Giménez-Saiz, C. J. Gómez-García and J. M. Fabre, *Synth. Met.*, 1999, **103**, 2279; M. Clemente-León, E. Coronado, J. R. Galán-Mascarós, C. J. Gómez-García and E. Canadell, *Inorg. Chem.*, 2000, **39**, 5394.
25 E. Coronado, J. R. Galán-Mascarós and C. J. Gómez-García, *J. Chem. Soc., Dalton Trans.*, 2000, 205; J. Peng, E. Wang, Y. Zhou, Y. Xing, H. Jia, Y. Lin and Y. Shen, *J. Chem. Soc., Dalton Trans.*, 1998, 3865; R. Kumai, M. Matsushita, A. Izuoka and T. Sugawara, *J. Am. Chem. Soc.*, 1994, **116**, 4523.